M. A. SOKOLOVSKIY
Water Problems Institute
Russian Academy of Sciences
3, Gubkina Str., GSP-1, 119991, Moscow, Russia
Institute of Mathematics and Mechanics
Ural Branch of the Russian Academy of Sciences
16, S. Kovalevskaja Str., GSP-384, 620219, Ekaterinburg, Russia
E-mail: sokol@aqua.laser.ru

J. VERRON
Laboratoire des Ecoulements Géophysiques er Industriels (LEGI)
UMR 5519, CNRS, BP53 X, 38041, Grenoble Cedex, France
E-mail: jacques.verron@inpg.fr

DYNAMICS OF THREE VORTICES IN A TWO-LAYER ROTATING FLUID

Received October 1, 2004 DOI: 10.1070/RD2004v009n04ABEH000288

The problem of studying the motion of three vortex lines with arbitrary intensities in an unbounded two-dimensional finite-thickness layer of a homogeneous fluid is known [25], [9], [28], [1] to belong to the class of integrable problems. However, a complete classification of possible motions was constructed only recently [10], [28], [41]. In [40], [39], [20] a generalization is given for *two-layer rotating fluid* in the particular case determined by the conditions of *(i)* zero total circulation of vortices, and *(ii)* the equality of the intensities of two vortices. Here, the first of these restrictions is lifted.

1. The governing equations

We suppose that the vortex motion takes place in an unbounded two-dimensional two-layer medium consisting of liquids with constant densities ρ_1, ρ_2 ($\rho_1 \leqslant \rho_2$) in the upper and lower layer, respectively. Suppose that the medium as a whole rotates around an axis perpendicular to the plane coinciding with the 'rigid' (by assumption) top boundary of the upper layer. Again, let one of the vortices be situated in the upper layer and two vortices in the lower layer.

The equations of motion in the coordinate system x, y rotating along with the medium with an angular velocity of Ω, take the form (see, e. g., [18], [20], [40])

$$u_1^1 = -\frac{1}{4\pi}\sum_{\alpha=1}^{2}\kappa_2^\alpha\frac{y_1^1-y_2^\alpha}{\left(r_{12}^{1\alpha}\right)^2}\left[1-\gamma r_{12}^{1\alpha}K_1\left(\gamma r_{12}^{1\alpha}\right)\right],$$

$$u_2^\alpha = -\frac{1}{4\pi}\left\{\kappa_2^{3-\alpha}\frac{y_2^\alpha-y_2^{3-\alpha}}{\left(r_{22}^{\alpha(3-\alpha)}\right)^2}\left[1+\gamma r_{22}^{\alpha(3-\alpha)}K_1\left(\gamma r_{22}^{\alpha(3-\alpha)}\right)\right]+\right.$$
$$\left.\kappa_1^1\frac{y_2^\alpha-y_1^1}{\left(r_{21}^{\alpha1}\right)^2}\left[1-\gamma r_{21}^{\alpha1}K_1\left(\gamma r_{21}^{\alpha1}\right)\right]\right\}, \tag{1.1}$$

Mathematics Subject Classification 37J35, 76B47, 76B70

$$v_1^1 = \frac{1}{4\pi}\sum_{\alpha=1}^{2}\kappa_2^\alpha\frac{x_1^1-x_2^\alpha}{\left(r_{12}^{1\alpha}\right)^2}\left[1-\gamma r_{12}^{1\alpha}K_1\left(\gamma r_{12}^{1\alpha}\right)\right],$$

$$v_2^\alpha = \frac{1}{4\pi}\left\{\kappa_2^{3-\alpha}\frac{x_2^\alpha-x_2^{3-\alpha}}{\left(r_{22}^{\alpha(3-\alpha)}\right)^2}\left[1+\gamma r_{22}^{\alpha(3-\alpha)}K_1\left(\gamma r_{22}^{\alpha(3-\alpha)}\right)\right]+\right.$$
$$\left.\kappa_1^1\frac{x_2^\alpha-x_1^1}{\left(r_{21}^{\alpha1}\right)^2}\left[1-\gamma r_{21}^{\alpha1}K_1\left(\gamma r_{21}^{\alpha1}\right)\right]\right\}. \tag{1.2}$$

Equations (1.1) and (1.2) are written in a dimensionless form with the assumption that the layers are of equal thickness ($h_1 = h_2 = 1/2$). Hereinafter, the superscript is the vortex number, and the subscript is the layer number (the layers are numbered from top to bottom); the numbers of vortices are denoted by Greek letters, and those of layers by Roman letters; $(x_j^\alpha,\, y_j^\alpha)$, $(u_j^\alpha,\, v_j^\alpha)$ and κ_j^α are (x,y)-coordinates, the components of velocity, and the intensity of the vortex $\binom{\alpha}{j}$,[1] respectively; $r_{ij}^{\alpha\beta} = \sqrt{\left(x_i^\alpha-x_j^\beta\right)^2+\left(y_i^\alpha-y_j^\beta\right)^2}$; $\gamma = 4\Omega/\sqrt{g(\rho_2-\rho_1)/\rho^*}$ is parameter of stratification; g is acceleration of gravity, ρ^* is mean density; $K_j(R)$ is the modified Bessel function of the j-th order of argument R.[2]

System of equations (1.1)–(1.2) has integral invariants:

$$Q = \frac{1}{2}\sum_{j=1}^{2}\sum_{\alpha=1}^{A_j}\kappa_j^\alpha \text{ — total intensity;}$$

$$P_x = \frac{1}{2}\sum_{j=1}^{2}\sum_{\alpha=1}^{A_j}x_j^\alpha\kappa_j^\alpha,\quad P_y = \frac{1}{2}\sum_{j=1}^{2}\sum_{\alpha=1}^{A_j}y_j^\alpha\kappa_j^\alpha \text{ — components of the total momentum;}$$

$$M = \frac{1}{2}\sum_{j=1}^{2}\sum_{\alpha=1}^{A_j}\left[\left(x_j^\alpha\right)^2+\left(y_j^\alpha\right)^2\right]\kappa_j^\alpha \text{ — total angular momenta.} \tag{1.3}$$

System of equations (1.1)–(1.2) can be written in the Hamiltonian form

$$\dot q_j^\alpha = \frac{\partial\mathcal{H}}{\partial p_j^\alpha} \equiv J\left(q_j^\alpha,\,\mathcal{H}\right),\qquad \dot p_j^\alpha = -\frac{\partial\mathcal{H}}{\partial q_j^\alpha} \equiv J\left(p_j^\alpha,\,\mathcal{H}\right),$$
$$j = 1,\,2,\quad \alpha = 1,\,A_j\ \ (A_1 = 1,\,A_2 = 2), \tag{1.4}$$

where J is the Jacobian operator, $q_j^\alpha = x_j^\alpha$ are generalized coordinates, $p_j^\alpha = y_j^\alpha\kappa_j^\alpha/2$ are generalized momenta, and

$$\mathcal{H} = -\frac{1}{4\pi}\sum_{j=1}^{2}\left\{\sum_{\substack{\alpha,\beta=1\\ \alpha\neq\beta}}^{A_j}\kappa_j^\alpha\kappa_j^\beta\left[\ln r_{jj}^{\alpha\beta}-K_0\left(\gamma r_{jj}^{\alpha\beta}\right)\right]+\right.$$
$$\left.+\sum_{\alpha,\,\beta=1}^{A_j,\,A_{3-j}}\kappa_j^\alpha\kappa_{3-j}^\beta\left[\ln r_{j(3-j)}^{\alpha\beta}+K_0\left(\gamma r_{j(3-j)}^{\alpha\beta}\right)\right]\right\} \tag{1.5}$$

is the Hamiltonian coinciding with the vortex interaction energy.

It is easy to verify that invariants M, $\mathcal{H}$ and the combination $(P_x)^2+(P_y)^2$ are pairwise involutory and hence, as was the case with a homogenous medium [9], [25], [1], [3], [4], [5], [11], [12], [13], [14], the problem of three vortices in a two-layer fluid always has a regular solution.

[1] Such notation will be used for a vortex with a number of α, concentrated in layer j (in this case, $\alpha = 1$ for $j = 1$ and $\alpha = 1,\,2$ for $j = 2$).

[2] Since the argument of the Bessel function depends not only on the distance between the vortices but also on the multiplicative constant γ, hereafter we will use denotations of the form $(X,\,Y) \equiv \gamma(x,\,y)$, $(X_j^\alpha,\,Y_j^\alpha) \equiv \gamma(x_j^\alpha,\,y_j^\alpha)$.

The specific features of the *absolute motion* of vortices will be studied below with the help of numerical solution of equations(1.1)–(1.2), supplemented by the appropriate initial conditions. The general properties of the *relative motion* are conveniently studied based on the qualitative analysis with the use of the so-called trilinear coordinates introduced in [1] and tested in [4], [6], [33], [34] and [40], [20], [38], [39], where they were applied to particular problems of three and four vortices in a homogeneous and a two-layer fluid, respectively.

2. Studying the relative and absolute motion of vortices

2.1. Phase portraits in trilinear coordinates

Following [1], let us consider a combination of integral invariants (1.3) in the form

$$L = QM - \left(P_x\right)^2 - \left(P_y\right)^2. \tag{2.1}$$

It is easy to show that L can be expressed in terms of squares of distances between the vortices, which allows this variable to be used for the analysis of the relative motion.

The trilinear coordinates (t_1, t_2, t_3), which at $L \neq 0$ satisfy the identity

$$t_1 + t_2 + t_3 = 3, \tag{2.2}$$

following from (2.1), in our case are introduced by the relationships

$$t_1 = \frac{3\kappa_2^1\kappa_2^2\left(r_{22}^{12}\right)^2}{L}, \qquad t_2 = \frac{3\kappa_1^1\kappa_2^2\left(r_{12}^{12}\right)^2}{L}, \qquad t_3 = \frac{3\kappa_1^1\kappa_2^1\left(r_{12}^{11}\right)^2}{L} \tag{2.3}$$

and characterize the distances from the coordinate lines $t_j = 0$, $(j = 1, 2, 3)$, constructed on the sides of an equilateral triangle with an altitude of 3, to any point on the plane (see figure 1a).

When $L = 0$, we have

$$t_1 + t_2 + t_3 = 0 \tag{2.4}$$

and

$$t_1 = 3\kappa_2^1\kappa_2^2\left(r_{22}^{12}\right)^2, \qquad t_2 = 3\kappa_1^1\kappa_2^2\left(r_{12}^{12}\right)^2, \qquad t_3 = 3\kappa_1^1\kappa_2^1\left(r_{12}^{11}\right)^2. \tag{2.5}$$

A geometric interpretation of the trilinear coordinates in this case is given in figure 1b.

In the case of a definite problem (when the initial coordinates of vortices and their intensities κ_j^α are specified) on the plane of variables (t_1, t_2, t_3), it is necessary to recognize the 'physical region' (PR), within which the triangle inequality holds for the distances between arbitrary three points. In terms of trilinear coordinates, this inequality takes the form

$$(\kappa_1^1 t_1)^2 + (\kappa_2^1 t_2)^2 + (\kappa_2^2 t_3)^2 \leqslant 2(\kappa_1^1\kappa_2^1 t_1 t_2 + \kappa_1^1\kappa_2^2 t_1 t_3 + \kappa_2^1\kappa_2^2 t_2 t_3). \tag{2.6}$$

Clearly, the points of the boundary of PR where (2.6) becomes an equality are always associated with a continuum of collinear states of the three vortices.

Eliminating t_1 from (2.2) and (2.4), we obtain, instead of (2.6), the following, more compact expressions

$$\left[\left(\kappa_1^1 + \kappa_2^1\right) t_2 + \left(\kappa_1^1 + \kappa_2^2\right) t_3 - 3\kappa_1^1\right]^2 \leqslant 4\kappa_2^1\kappa_2^2 t_2 t_3 \tag{2.7}$$

and

$$\left[\left(\kappa_1^1 + \kappa_2^1\right) t_2 + \left(\kappa_1^1 + \kappa_2^2\right) t_3\right]^2 \leqslant 4\kappa_2^1\kappa_2^2 t_2 t_3 \tag{2.8}$$

for the cases $L \neq 0$ and $L = 0$, respectively.

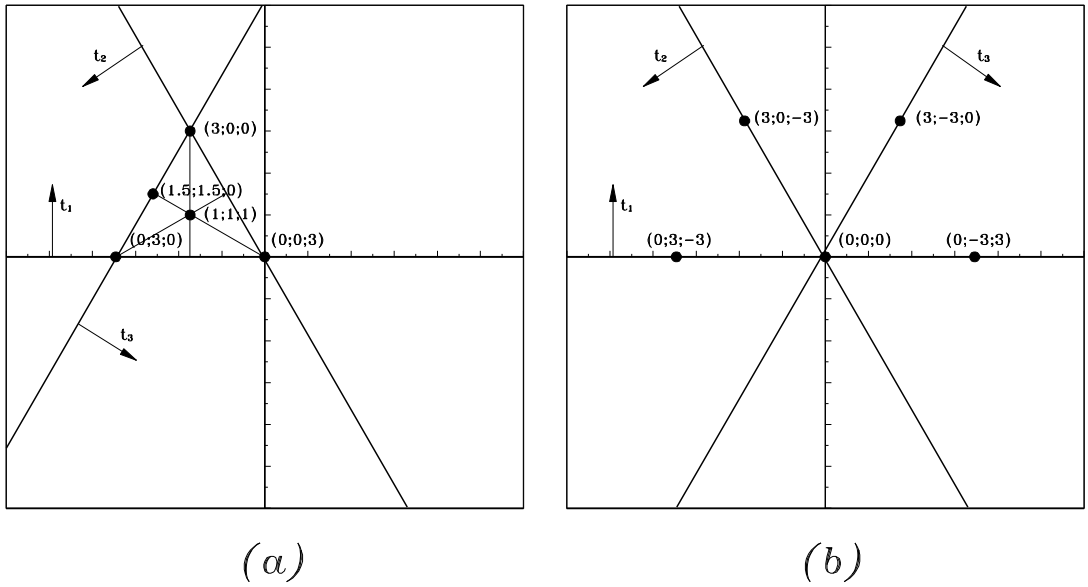

Fig. 1. Scheme of trilinear coordinates and axes orientation at $L \neq 0$ — *(a)* and $L = 0$ — *(b)*.

Isolines of the Hamiltonian (1.5), expressed in terms of trilinear coordinates are phase portraits of the relative motion of the vortex structure within the PR.

In the case of $\kappa_2^1 = \kappa_2^2 = \kappa$; $\kappa_1^1 = \mu\kappa$ (μ is an arbitrary parameter) considered here, we have from (2.1)

$$\frac{L}{\kappa^2} = \mu\Big[\Big(r_{12}^{11}\Big)^2 + \Big(r_{12}^{12}\Big)^2\Big] + \Big(r_{22}^{12}\Big)^2, \tag{2.9}$$

from where it follows that variable L can change its sign only at

$$0 > \mu = -\frac{\Big(r_{22}^{12}\Big)^2}{\Big(r_{12}^{11}\Big)^2 + \Big(r_{12}^{12}\Big)^2} > -2, \tag{2.10}$$

while at $\mu \leqslant -2$ and $\mu > 0$, L sign is negative in the first case and positive in other.

The condition (2.7) for the trilinear coordinates to belong to PR now takes the form

$$\big[(\mu+1)(t_2+t_3) - 3\mu\big]^2 \leqslant 4t_2t_3, \tag{2.11}$$

from where it readily follows that at $\mu \geqslant 1$ and at $\mu < -2$, all PR are compact and hence the relative motions are finite on finite carriers. In the interval $\mu \in [-2;\, 1)$, PR are infinitary.

Figures 2–5 demonstrate a series of phase portraits at different fixed values of μ and L.

Three examples of phase portraits of compact type for the specified values of μ are given in figure 2. The PR in figures 2a, 2b and 2c are determined by the conditions

$$\begin{gathered}
\Big(t_2+t_3-5\Big)^2 \leqslant \frac{16}{9}t_2t_3, \quad t_1 \leqslant 0;\ t_2,\, t_3 \geqslant 0 \quad \text{at} \quad \gamma^2 L = -5,\ \mu = -2.5; \\
\Big(t_2+t_3-\frac{3}{2}\Big)^2 \leqslant t_2t_3, \quad t_1 \geqslant 0;\ t_2,\, t_3 \leqslant 0 \quad \text{at} \quad \gamma^2 L = 2,\ \mu = 1; \\
\Big(t_2+t_3-2\Big)^2 \leqslant \frac{4}{9}t_2t_3, \quad t_1 \geqslant 0;\ t_2,\, t_3 \leqslant 0 \quad \text{at} \quad \gamma^2 L = 2,\ \mu = 2,
\end{gathered} \tag{2.12}$$

respectively. PR of noncompact type in figure 3 are described by relationships

$$\Big(t_2+t_3-9\Big)^2 \leqslant 16t_2t_3, \quad \begin{cases} t_1 \leqslant 0; \quad t_2,\, t_3 \geqslant 0;\ L < 0 \\ t_1 \geqslant 12;\ t_2,\, t_2 < 0;\ L > 0 \end{cases} \quad \text{at} \quad \mu = -1.5; \tag{2.13}$$

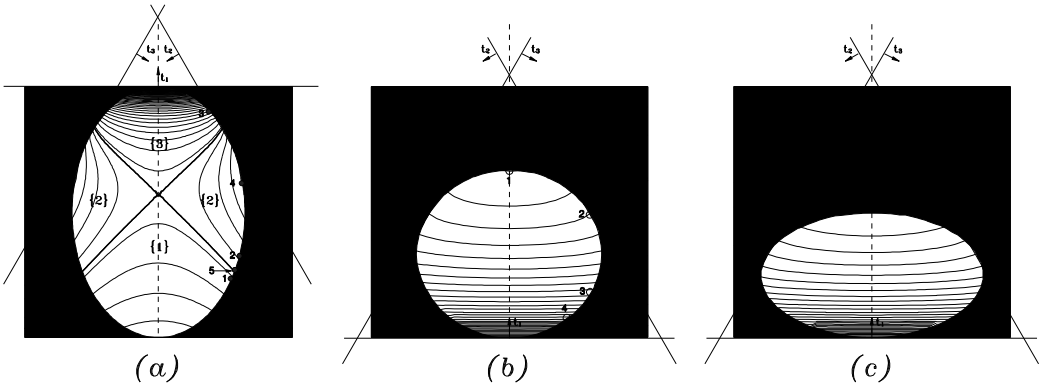

Fig. 2. Phase portraits (compact case) for three-vortex problems in trilinear coordinates in PR (2.12): $\gamma^2 L = -5$, $\mu = -2.5$ — *(a)*; $\gamma^2 L = 2$, $\mu = 1$ — *(b)*; $\gamma^2 L = 2$, $\mu = 2$ — *(c)*. The thick lines in fragment *(a)*, as before, are separatrices dividing the domains of existence of different types of solutions {1}, {2} and {3}; their properties will be discussed in paragraphs 2.3 and 2.4. Figures denote the boundary points of PR that correspond to the initial conditions for numerical experiments, the results of which are given in figures 11, 12, 14.

in figure 4, by relationships

$$t_2 t_3 \geqslant \frac{9}{4}, \quad \begin{cases} t_1 < 0; \quad t_2,\, t_3 \geqslant 0;\ \gamma^2 L = -2 \\ t_1 \geqslant 6; \quad t_2,\, t_2 < 0;\ \gamma^2 L = 2 \end{cases} \quad \text{at} \quad \mu = -1; \tag{2.14}$$

and in figures 5a and 5b (where $L = 0$):

$$\begin{aligned} &\Big(t_2 + t_3 - 9\Big)^2 \leqslant 16 t_2 t_3, \quad t_1 \geqslant 0;\ t_2,\, t_3 < 0 \quad \text{at} \quad \mu = -1.5; \\ &\Big(t_2 + t_3 + 3\Big)^2 \leqslant 16 t_2 t_3, \quad t_1 \geqslant 0;\ t_2,\, t_3 < 0 \quad \text{at} \quad \mu = -0.5. \end{aligned} \tag{2.15}$$

Note on choreographies. Of great importance in the celestial mechanics and the theory of vortices are closed trajectories, which correspond to periodic solutions of the problem. Running a few steps forward, we note that, in the interpretation of the relative motion of vortices with the use of the trilinear coordinates, periodic motions are clearly distinguishable, because the respective phase curves begin and end on the PR boundary. The respective trajectories of vortices (or material bodies) are referred to as *choreographies* [36], [37], [35], [10].

Although the solution of the three-body problem in the form of a closed circular trajectory was first obtained by Lagrange as far back as 1772 [35], and later, starting from works of Hénon [23] and Moore [29], the class of available solutions (for problems of celestial mechanics with a uniform Newtonian potential) with closed trajectories had extended significantly, the notion of *choreography* was coined by Simó [36] quite recently (2002).

Choreographies can be

- *absolute* when the trajectories are closed in a fixed coordinate system;
- *relative* when the trajectories become closed in a coordinate system rotating uniformly around a centre of rotation (or moving with a constant translational velocity, if the centre of rotation lies at infinity);
- *simple* when all the bodies (or vortices) move along the same trajectory; and
- *complex* when at least one body moves along a trajectory of its own.

First attempts to apply the notion of choreography to vortex dynamics in a homogenous fluid on a plane and a sphere were made by Borisov, Mamaev, and Kilin in [10], [15].

Taking into account the two-layer character of the vortex structures considered in this study, the problem of distinguishing choreographies becomes even more important. As will be shown below, there can be situations in two-layer media when the vortices belonging to different layers have common trajectories. We will not study choreographies systematically but will repeatedly mention the cases of existence of this special class of vortex motions.

The patterns of phase portraits (figures 2–5) demonstrate a wide diversity of their topological properties. A detailed discussion of some of them given below in connection with specific problems will be accompanied by demonstrations of absolute trajectories of vortices and their relative choreographies. However, first we will obtain the conditions of existence of singular points on the phase plane, which correspond to stationary solutions of the equations of motion (1.1)–(1.2).

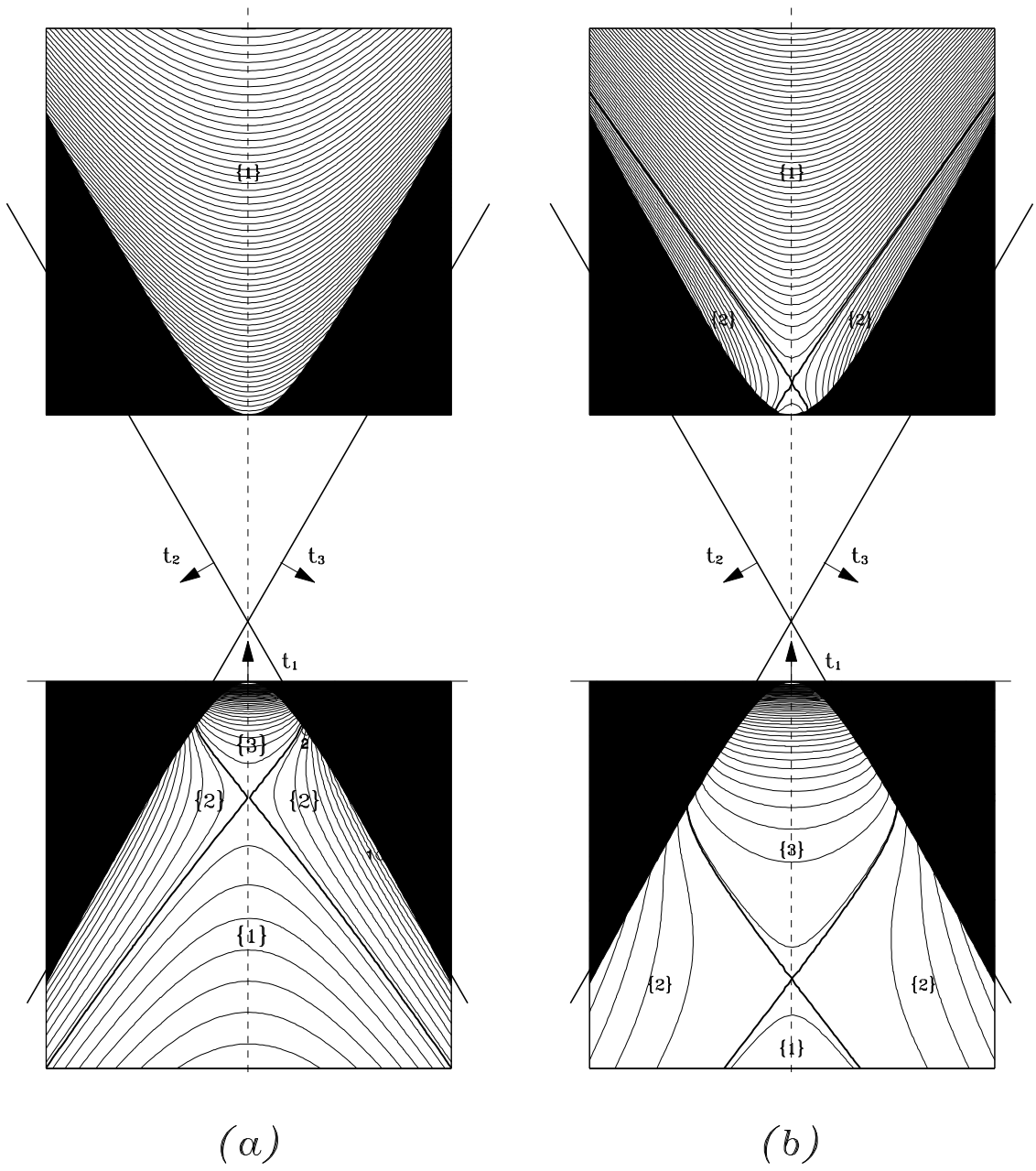

Fig. 3. Phase portraits of three-vortex problems in PR (2.13) at $\mu = -1.5$ and $L < 0$ — in the lower part, $L > 0$ — in the upper part: $\gamma^2|L| = 2$ — *(a)*; in the lower part $\gamma^2|L| = 0.65$ — *(b)*. Figures mark the points in PR that correspond to the initial conditions for the experiments the results of which are given in figure 13.

2.2. Analysis of stationary states

Judging from figures 2–5, we can conclude that two types of singular points — stable elliptic and unstable hyperbolic — can appear in the problems of the class considered here. The former always belong to the boundary of PR, and the latter coincide with the self-intersection points of separatrices. Both elliptic and hyperbolic singularities are obviously associated with rotational motions of rigid configurations of three vortices — collinear in the former case, and isosceles-triangular in the latter case. These rotations take place around the vorticity center of the vortex structure, which has the coordinates

$$(X_c,\, Y_c) = \left(\frac{\gamma P_x}{Q},\, \frac{\gamma P_y}{Q}\right). \tag{2.16}$$

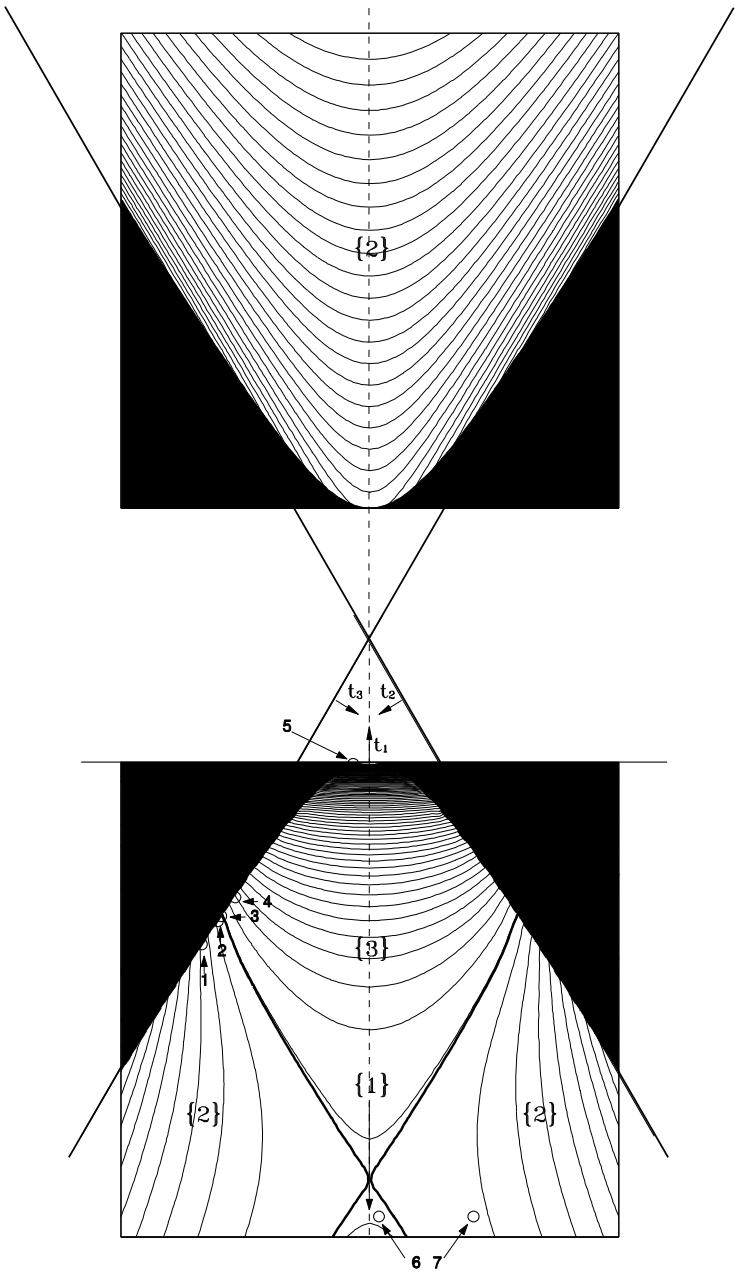

Fig. 4. Phase portraits of three-vortex problems in PR (2.14) at $\mu = -1$ and $\gamma^2 L = -2$ — in the lower part, $\gamma^2 L = 2$ — in the upper part. Figures mark the points in PR that correspond to the initial conditions for the experiments the results of which are given in figure 15.

The boundary elliptic singular points are also divided into *polar* — in the upper and (or) lower parts of the PR for finite (infinite) PR — and *side* points. If for a polar point we have $t_1 = 0$, it corresponds to a structure comprising an upper-layer vortex and theoretically merged lower-layer vortices; otherwise, if $t_1 \neq 0$, this point corresponds to an *ordinary* or *inverse roundabout*. Of particular interest is the existence of side elliptic points, which are phase prototypes of *eccentric roundabouts*[3].

[3]The terms *ordinary* and *inverse roundabouts* are introduced in [38] to define rigid axisymmetric triangular structures for which the peripheral vortices of the lower layer rotate with respect to the central vortex in the upper layer in the direction induced by this vortex or in the direction determined by the intralayer interaction, respectively. The *ordinary roundabout* is a two-layer analogue of the so-called tripolar vortices or tripoles in a homogeneous fluid [8], [17], [21], [22], [24], [31], [42]; *inverse roundabout* has a purely baroclinic nature. The term *eccentric roundabout* is assigned in [38] to

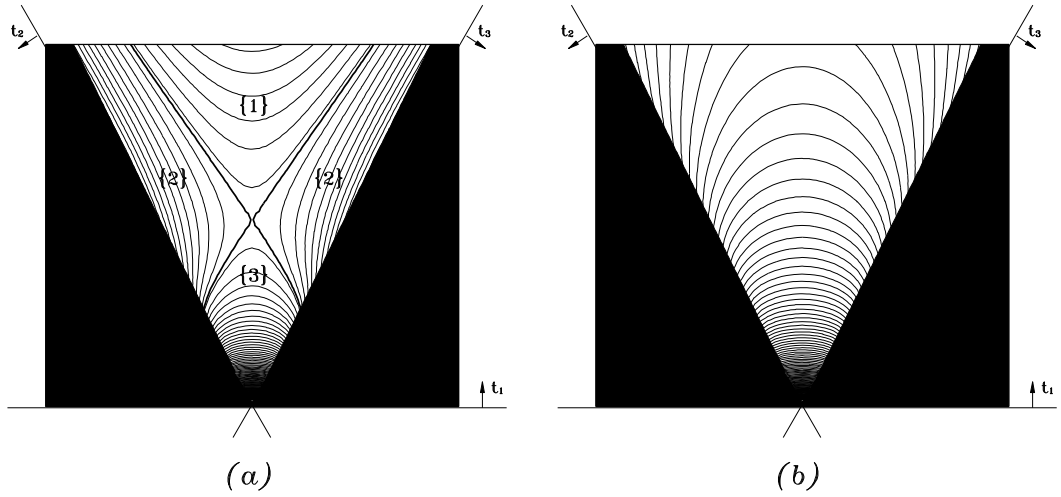

Fig. 5. Phase portraits of three-vortex problems in PR (2.15) at $L = 0$: $\mu = -1.5$ — *(a)* and $\mu = -0.5$ — *(b)*.

We have

$$(X_c,\, Y_c) = \begin{cases} \left(\dfrac{2(R-B)}{\mu+2},\, 0\right) & \text{for side elliptical singular points;} \\ \left(0,\, \dfrac{2B\sin\varphi}{\mu+2}\right) & \text{for hyperbolic singular points.} \end{cases} \tag{2.17}$$

The meaning of variables B, R and φ, where $\varphi \in [0;\, \pi/2)$, is clarified by figures 6a, 7a, 9a and 10a, where, without loss of generality, it is assumed that, in the initial moment, the upper layer vortex $\binom{1}{1}$ localizes in the origin of coordinates $(X,\, Y) = (0,\, 0)$, and

(i) the collinear configuration belongs to the X-axis, and

(ii) the triangular configuration is symmetrical about the Y axis.

For collinear configurations, we obviously have

$$\begin{array}{lllll} X_c \geqslant 0 & \text{at} & \mu < -2,\, B \geqslant R & \text{or} & \mu > -2,\, B \leqslant R, \\ X_c \leqslant 0 & \text{at} & \mu > -2,\, B \geqslant R & \text{or} & \mu < -2,\, B \leqslant R, \end{array} \tag{2.18}$$

and for triangular configurations,

$$\begin{array}{lll} Y_c \geqslant 0 & \text{at} & \mu > -2, \\ Y_c \leqslant 0 & \text{at} & \mu < -2. \end{array} \tag{2.19}$$

At $\mu \to -2$ (when the total intensity equals zero) the vorticity center tends to an infinite point[4].

Let us consider some interesting particular combinations of coordinates (2.17).

- For the collinear structure, the vorticity center
  - belongs to the center of the segment between vortices $\binom{1}{2}$ and $\binom{2}{2}$ at $\mu = 0$;
  - coincides with vortex $\binom{2}{2}$ at $\mu \neq 0$ and

$$B = \frac{2R(1+\mu)}{\mu}; \tag{2.20}$$

an *axisymmetric* structure for which the center of rotation does not coincide with the central vortex. In this work, the latter definition is generalized to the *asymmetric* case.

[4]This case is studied in [38].

– coincides with the center of the segment between vortices $\binom{1}{1}$ and $\binom{2}{2}$ at $\mu \neq 2$ and

$$B = \frac{2R\mu}{\mu - 2}. \tag{2.21}$$

- For the triangular structure, the vorticity center
  - lies within the triangle formed by the vortices at $\mu > 0$;
  - lies outside this triangle at $\mu < 0$, and, as mentioned above, at $\mu = -2$ — it moves to infinity;
  - coincides with the center of the circle circumscribed around this triangle at $\mu = -2\cos 2\varphi$; the center of this circle, in its turn, lies within the triangle at $\varphi > \pi/4$ (when $0 < \mu < 2$) and outside the triangle at $\varphi < \pi/4$ (when $-2 < \mu < 0$).

We obtain dispersion equations describing the conditions of existence of steady-state solutions either of collinear type in the form of an eccentric roundabout or in the form of an isosceles triangle.

2.2.1. Eccentric roundabout

Using equations (1.1)–(1.2), we readily obtain the dispersion equation for a steady state configuration in the form of a uniformly rotating collinear structure:

$$F(B,\, R;\, \mu) = \frac{1}{2} + \frac{2R(1+\mu)}{B(2R-B)} + K_1(2R) - \frac{(2R + B\mu)K_1(2R-B) + [2R(1+\mu) - B\mu]K_1(B)}{2(R-B)} = 0. \tag{2.22}$$

Clearly, F is a monotonically decreasing function of both B and R, and

$$F \sim \begin{cases} 1/\varepsilon_1 > 0,\ \varepsilon_1 = \min(B,\, R) \quad \text{at} \quad B,\, R \ll 1; \\ (1+\mu)\big[1/\varepsilon_2 - K_1(\varepsilon_2)\big],\ \varepsilon_2 = B \ll 1 \quad \text{at} \quad R \gg 1; \\ (1+\mu)\big[1/\varepsilon_3 - K_1(\varepsilon_3)\big],\ \varepsilon_3 = 2R - B \ll 1 \quad \text{at} \quad B \to 2R,\ R \gg 1. \end{cases} \tag{2.23}$$

Expressions in square brackets in (2.23) are always positive; therefore, the necessary condition for the existence of solution of equation (2.22) can be written as the inequality

$$\mu < -1. \tag{2.24}$$

Thus, the coordinates of the center of rotation for *stationary states in the form of an eccentric roundabout* correspond to a narrower interval of parameter μ than that specified by (2.18) for *arbitrary collinear configurations*. Namely:

$$\begin{array}{l} X_c \geqslant 0 \quad \text{at} \quad \mu < -2,\ B \geqslant R \quad \text{or} \quad -1 > \mu > -2,\ B \leqslant R, \\ X_c \leqslant 0 \quad \text{at} \quad -1 > \mu > -2,\ B \geqslant R \quad \text{or} \quad \mu < -2,\ B \leqslant R. \end{array} \tag{2.25}$$

The angular velocity of the rectilinear vortical structure with respect to the vorticity center (2.25) is

$$\omega = \frac{\gamma\kappa(\mu+2)}{4\pi(2R + B\mu)}\left[\frac{B + 2R\mu}{2BR} - \mu K_1(B) + K_1(2R)\right]. \tag{2.26}$$

The case $\mu = -2$ (i. e. $Q = 0$), when the angular velocity becomes zero, and the rotation center (2.17) moves to an infinite point, was studied in [38].

Figures 6 and 7 demonstrate the character of solution to equation (2.22) at $\mu = -2.5$ and $\mu = -1.5$, respectively, within a wide range of values of integral L. In particular, they show the above-mentioned property that the sign of L is constant at $\mu \leqslant -2$ and can change at $0 > \mu > -2$. Note that curve $X_c(R)$ is symmetrical with respect to the R axis, and $B(R)$ is symmetrical with respect to straight line $B = R$, and with growing R, the value of B asymptotically approaches 0 or $2R$ at $R > B$ and $R < B$, respectively — see (2.23). To illustrate these effects, auxiliary half-rays $B = R$ and $B = 2R$ are shown in the figures by dotted lines. Obviously, at $R \to \infty$, the angular velocity tends to zero.

The motion of vortices in the cases when both the dispersion equation (2.22) and the relationships (2.20) or (2.21) are valid is illustrated in figure 8. Here and in all subsequent figures, where vortex trajectories (or choreographies) are shown, triangular markers denote the instantaneous positions of the upper-layer vortex, and circle and box markers denote the positions of the lower-layer vortices. The rotation in figure 8a is cyclonic, and the center of vorticity coincides with the vortex $\binom{2}{2}$, while the rotation in figure 8b is anticyclonic and the trajectories of vortices $\binom{1}{1}$ and $\binom{1}{2}$ coincide (the calculation, however, was terminated before they begin to overlap). Clearly, the collinearity condition for configuration is valid everywhere in this case, but the segments passing through three vortices are shown in the figure only for two time moments for each experiment, i.e., the initial (when the vortices lie on the X-axis) and the final (target).

2.2.2. Triangular stationary structure

Similarly, we can obtain relationships between the geometrical parameters of a stationary unstable vortex structure in the form of a uniformly rotating isosceles triangle (figures 9 and 10), which corresponds to a fixed hyperbolic singular point of the phase portrait.

The dispersion equation relating the side length of triangle B and the angle at its base φ has the form

$$\frac{1 + 2B\cos\varphi K_1(2B\cos\varphi)}{\cos^2\varphi} = -4(1+\mu)\big[1 - BK_1(B)\big]. \tag{2.27}$$

Since the expression in the left-hand part of (2.27) is always greater than unity and $0 < 1 - BK_1(B) < 1$, the necessary condition for the existence of solution to the dispersion equation takes the form

$$\mu < -5/4. \tag{2.28}$$

It is worth mentioning here that the comparison of conditions (2.24) and (2.28) yields the explanation of the fact that at $\mu = -1$ (figure 4), there are no side elliptic singular points, while there is a hyperbolic singular point.

The asymptotic properties of modified Bessel functions [32] determine the restrictions on the angle at the base of the triangle at $B \gg 1$:

$$\arccos\varphi < \sqrt{-\frac{1}{4(1+\mu)}}. \tag{2.29}$$

clearly, the values of parameter μ should lie on the half-line (2.28) on which the expression under the radical in (2.29) is always positive.

Formula for the angular velocity of the triangular structure relative to the vorticity center $(0, Y_c)$ takes the form

$$\omega = \frac{\gamma\kappa(2+\mu)}{4\pi B^2}\Big[1 - BK_1(B)\Big]. \tag{2.30}$$

If $\kappa > 0$, it becomes $\omega \leqslant 0$ at $\mu \leqslant -2$, and, in view of (2.28), $\omega \geqslant 0$ at $-5/4 > \mu \geqslant -2$.

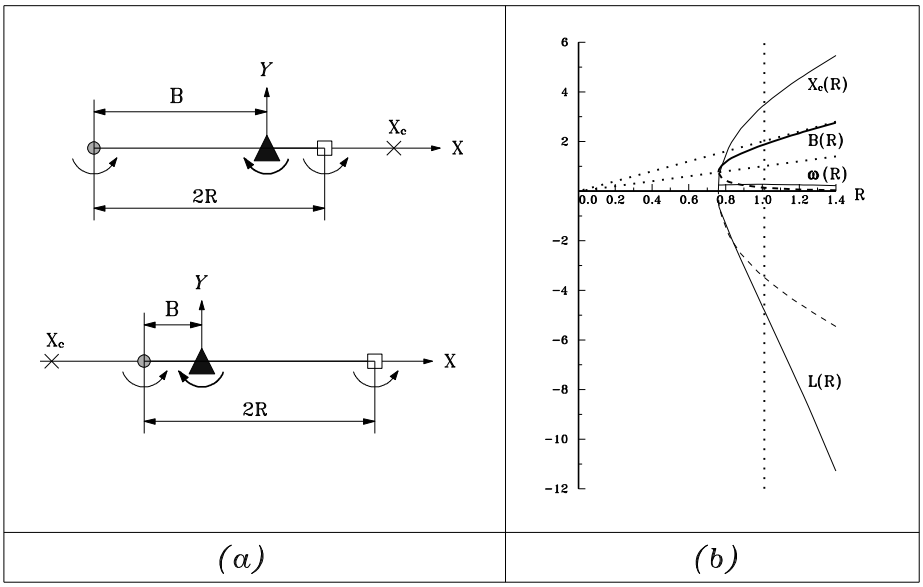

Fig. 6. Scheme of the initial position of vortices for an *eccentric roundabout* at $B > R$ (top) and at $B < R$ (bottom) — *(a)*; dispersion curve $B(R)$, satisfying (2.22), the curve of coordinates of the vorticity center $X_c(R)$, the angular velocity (2.26) of rotation of the vortex construction $\omega(R)$ and the value of the integral invariant $L(B)$ (2.9) at $\mu = -2.5$ — *(b)*. The tilted dashed lines have equations $B = R$ and $B = 2R$. The branches of curves $B(R)$ and $X_c(R)$ for the case $B > R$ are shown by the full line, and those for $B < R$ by the dashed line. The points of intersection of the curves with the vertical dashed line correspond to the parameters of numerical experiments at $\gamma^2 L = -5$, shown in figure 12a.

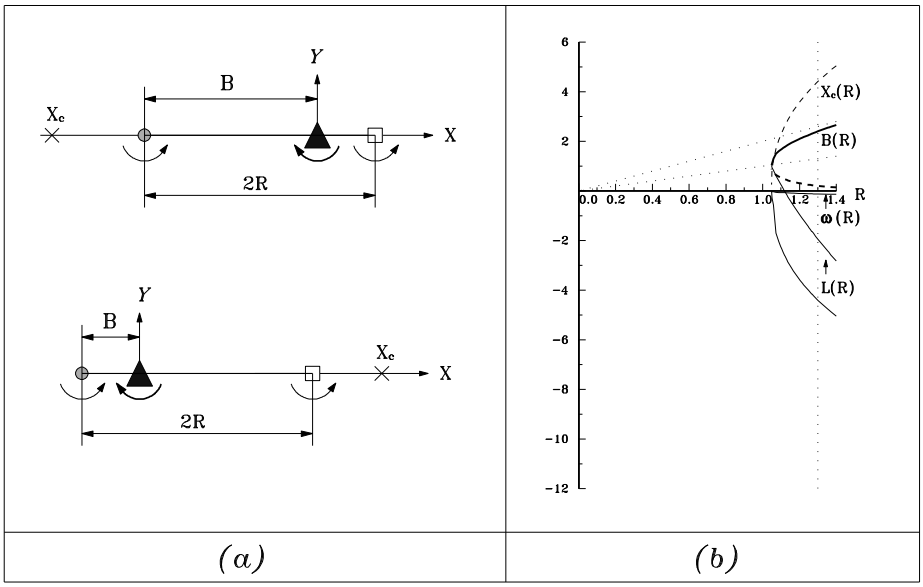

Fig. 7. The same as in figure 6 but for $\mu = -1.5$. The points of intersection of the curves with the vertical dashed line correspond to the parameters of numerical experiments at $\gamma^2 L = -2$, shown in figure 13a.

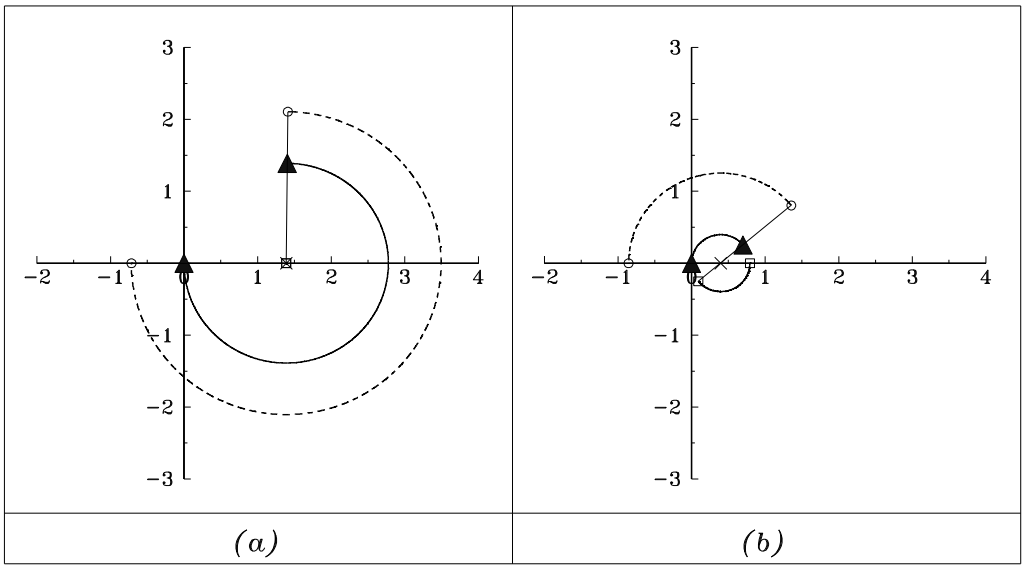

Fig. 8. Trajectories of absolute motion of vortex structures — *eccentric roundabouts* — in the case when the conditions (2.20) — *(a)* and (2.21) — *(b)* are satisfied. Parameter values: $\mu = -1.5757$, $B = 0.7162$, $R = 1.0526$, $L = 0.5746$ — *(a)*; $\mu = -2.1598$, $B = 0.8551$, $R = 0.8235$, $L = -0.2211$ — *(b)*. The full curves represent the upper-layer vortex trajectories $\binom{1}{1}$, and the dashed line, those of the lower-layer vortices $\binom{1}{2}$ and $\binom{2}{2}$.

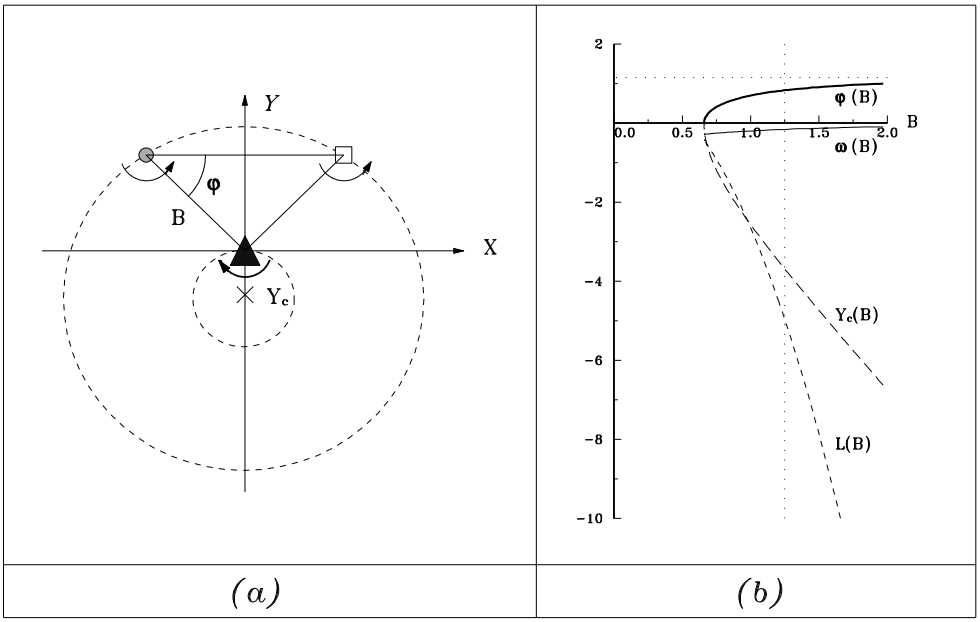

Fig. 9. Scheme of the initial distribution of vortices for a rigidly rotating vortex structure in the form of an isosceles triangle at $\mu = -2.5$. The dashed lines represent the theoretical trajectories of vortices — *(a)*. The respective dispersion curve $\varphi(R)$ (thick full line), satisfying (2.27), the angular velocity (2.30) of rotation of the vortex structure $\omega(R)$ (thin full line), the curve of coordinates of the vorticity center $Y_c(R)$ (long dashes), and the value (2.9) of the integral invariant $L(B)$ (short dashes) — *(b)*. The horizontal dashed line is an asymptote (2.29) for $\varphi(R)$, and the vertical line marks, on the curves, the values of functions corresponding to experiments in the figure 12b.

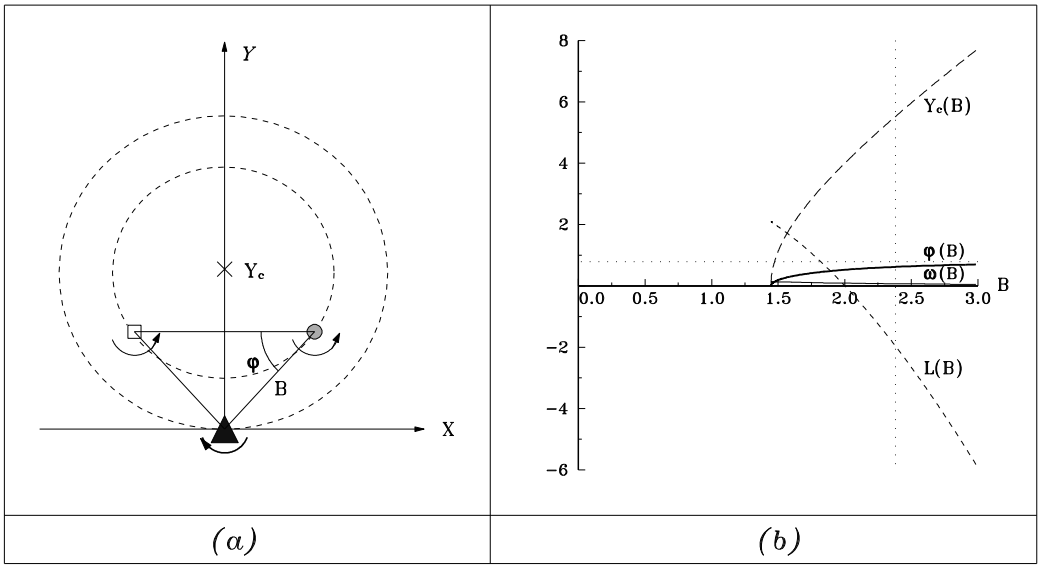

Fig. 10. The same as in figure 9, but at $\mu = -1.5$. The vertical dashed line reflects the parameters of experiments in figure 13b.

2.3. Classification of motions of triangular vortical structures

In this paragraph, we will discuss the features of different types of motion of vortices based, on the one hand, on the classification provided by phase portraits in figures 2–5, and, on the other hand, on studying the behavior of trajectories of the absolute motion of vortices and their relative choreographies by numerically solving the equations of motion (1.1)–(1.2).

The choice of the initial conditions in the numerical experiments coordinated with the analysis of phase portraits will be based on the following considerations.

(i) If the phase curves of the class of motions considered reach the boundary of PR and, thus, the set of possible vortex configurations contains a collinear structure, we will suppose that all the three vortices belong to the X-axis, the vortex $\binom{1}{1}$ localizes in the origin, and the coordinates of vortices $\binom{1}{2}$ and $\binom{2}{2}$ satisfy the conservation condition of the invariant L, i. e., at $t = 0$,

$$X_1^1 = Y_1^1 = Y_2^1 = Y_2^2 = 0;$$

$$X_2^1 = \begin{cases} \dfrac{X_2^2 - \sqrt{\left(X_2^2\right)^2\left[1-(1+\mu)^2\right] + \gamma^2 L(1+\mu)}}{1+\mu} & \text{at} \quad \mu \neq -1, \\ -\dfrac{\gamma^2 L}{X_2^2} \quad \text{at} \quad \mu = -1. \end{cases} \tag{2.31}$$

(ii) If the phase trajectories do not reach the boundary of PR, we will assume that at $t = 0$, only vortices $\binom{1}{1}$ and $\binom{1}{2}$ belong to the X-axis, and the vortex $\binom{2}{2}$ does not belong to it:

$$X_1^1 = Y_1^1 = Y_2^1 = 0;$$

$$X_2^1 = \begin{cases} \dfrac{X_2^2 - \sqrt{\left(X_2^2\right)^2\left[1-(1+\mu)^2\right] - (1+\mu)^2\left(Y_2^2\right)^2 + \gamma^2 L(1+\mu)}}{1+\mu} & \text{at} \quad \mu \neq -1, \\ -\dfrac{\gamma^2 L}{X_2^2} \quad \text{at} \quad \mu = -1. \end{cases} \tag{2.32}$$

Bearing in mind (2.31)–(2.32), when specifying the parameters of the initial state in the captions to figures showing vortex trajectories, we will show only the values of the X_2^2 coordinate in the first case, and the pair of coordinates (X_2^2, Y_2^2) in the second case.

Analysis of the phase portraits in figures 2–5 shows that, at least in this (relatively wide) interval of external parameters, no more than three qualitatively different types of motion are possible:

- Type {1} — double trapping, when all three vortices are involved in joint rotational motion in the direction induced either by their resultant intensity or by the intensity of the 'strongest' vortex. This motion can be conventionally determined by the scheme:

$$\binom{1}{1}\binom{1}{2}\binom{2}{2}. \tag{2.33}$$

- Type {2} — simple trapping, when one of the lower-layer vortices combines with the upper-layer vortex and one of the following formulas is valid:

$$\binom{1}{1}\binom{1}{2}+\binom{2}{2} \qquad \text{or} \qquad \binom{1}{1}\binom{2}{2}+\binom{1}{2}. \tag{2.34}$$

- Type {3} — the interaction between the two lower-layer vortices predominates, and the motion is determined by the scheme

$$\binom{1}{2}\binom{2}{2}+\binom{1}{1}. \tag{2.35}$$

2.4. Absolute motion of vortices. Choreographies

Analysis of the relative motion of vortex structures is known to be unable to yield a complete picture of their actual dynamics. In this paragraph, in addition to the above-considered specific cases of vortex motion trajectories under stationary conditions, we will discuss in greater detail the features of the absolute motion of triangular vortex structures in combination with the qualitative analysis based on some of figures 2–5.

Characteristic examples of trajectories of all three types of absolute motion and the respective relative choreographies at $\mu = -2.5$ are given in figure 11,[5] where, obviously, the choreographies are plotted in the system of coordinates uniformly rotating around the vorticity center in the anticyclonic direction. It is worth mentioning that, on the relative choreographies of motions of types {1} and {3}, the lower-layer vortices $\binom{1}{2}$ and $\binom{2}{2}$ move along the same trajectory, always remaining on the opposite ends of its 'diameter'. However, in the first case, they (in a moving coordinate system) move along closed trajectories in the clockwise direction induced by the upper-layer vortex; in the second case, because of the predominance of intralayer interaction, they move in the opposite direction (formulas (2.33), (2.35)). For motions of type {1}, vortex $\binom{1}{1}$ stays within the closed figure described by the lower-layer vortices, and for motions of type {3}, outside this figure.

Figures 12a-13a illustrate in more detail the interaction of type {2} for the cases when the image point of the phase plane coincides with the side elliptic point and we have a stable rotation of a rigid collinear structure, i.e., an eccentric roundabout. Figures 12b-13b demonstrate the unstable character of the triangular construction (the respective phase trajectory lies in the vicinity of the separatrix): the vortices alternately either occupy the vertices of the isosceles triangle or lie along a straight line, as the image point moving along the phase curve lies either in a vicinity of the hyperbolic singularity or on the boundary of PR, respectively. It is worth mentioning that the relative choreographies in figure 12 have been obtained in the coordinate system rotating around the vorticity center with a negative angular velocity as $\mu < -2$ (see the formula for angular velocity (2.26)), and those in figure 13, where $\mu > -2$, with a positive velocity[6].

[5] Hereafter, in the captions to the figures where absolute trajectories are shown, we will use denotations of the form $t = (t_1, t_2, t_3)$ to specify the initial coordinates of the respective image points on the phase plane.

[6] See also the behavior of curves $\omega(B)$ in figures 9 and 10.

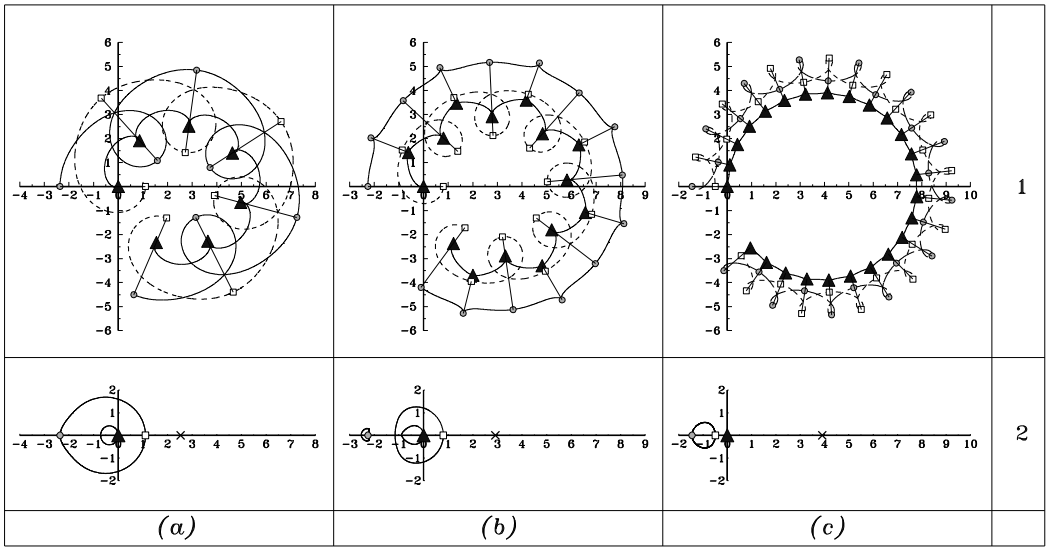

Fig. 11. Trajectories of absolute motion — 1 and the respective choreographies — 2 for motions of the types{1} — *(a)*, {2} — *(b)*, {3} — *(c)* at $\gamma^2 L = -5$, $\mu = -2.5$ and the initial conditions specified by formulas (2.31) with $X_2^2 = 1.1$, $t = (-7.2022;\ 1.8150;\ 8.3872)$ — *(a)*; $X_2^2 = 0.8$, $t = (-5.6143;\ 0.9600;\ 7.6543)$ — *(b)*, $X_2^2 = -0.5$, $t = (-0.5460;\ 0.3750;\ 3.1710)$ — *(c)*. The markers spaced a half-period apart and the segments connecting them show synchronous (collinear) positions of vortices. The initial trilinear coordinates for the cases *(a)*, *(b)* and *(c)* correspond to points with the numbers 1, 2 and 3 in figure 2a. Crosses on the X-axis in the lower part of the figure show the coordinates of the vorticity centers $(X_c,\ 0)$.

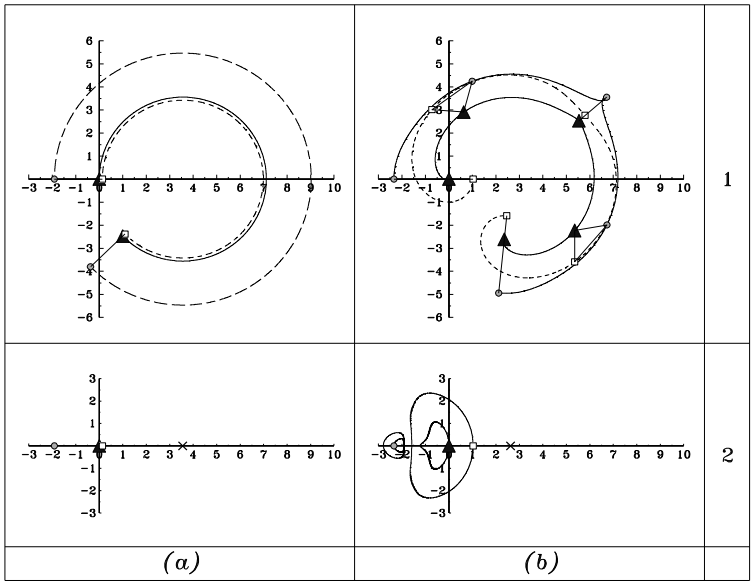

Fig. 12. The same as in figure 11 for motions of the type {2} at the initial conditions with $X_2^2 = 0.13233$, $t = (-2.5058;\ 0.0263;\ 5.4796)$ — *(a)*; $X_2^2 = 1.02777$, $t = (-6.8150;\ 1.5845;\ 8.2305)$ — *(b)*. The trilinear initial coordinates for the cases *(a)* and *(b)* correspond to points with numbers 4 and 5 in figure 2a — in the elliptic point and in a vicinity of the point where the separatrix reaches the PR boundary, respectively.

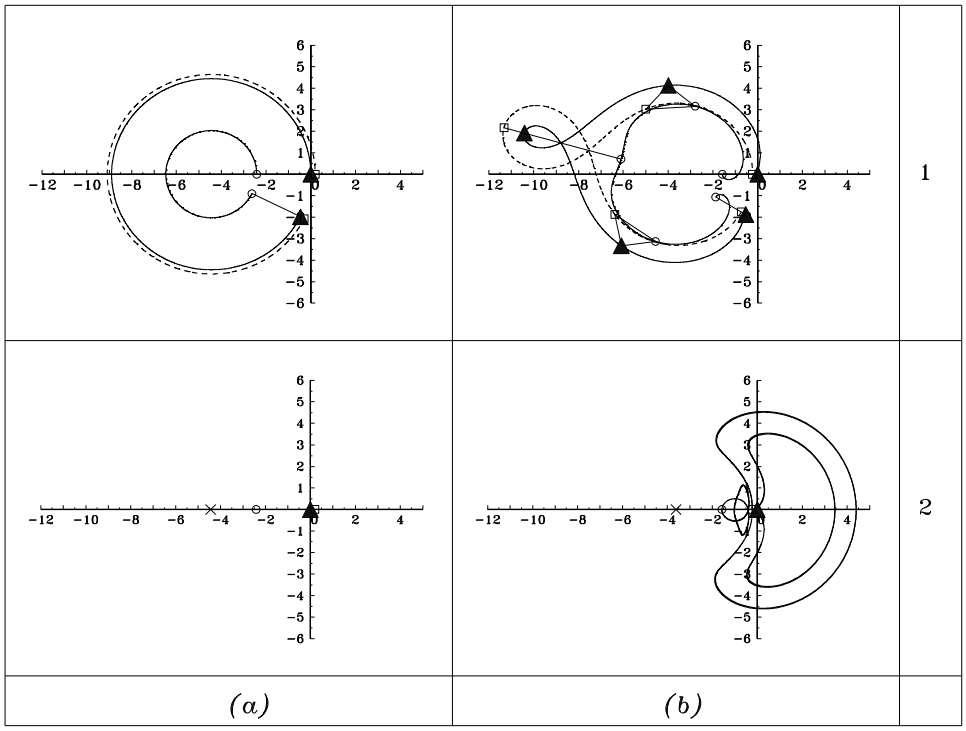

Fig. 13. Trajectories of the absolute motion — 1 and the respective choreographies — 2 for motions of type {2} at $\gamma^2 L = -2$, $\mu = -1.5$ and the initial conditions with $X_2^2 = 0.1949$, $t = (-10.2416;\ 0.0855;\ 13.1561)$ — *(a)*; $X_2^2 = -0.2338$, $t = (-2.6901;\ 0.1230;\ 5.5671)$ — *(b)*. Rectilinear segments in figure *(a)* show the collinear positions of vortices in the initial and final time moments in the calculation, and in figure *(b)*, at intervals of a quarter of period (the configurations are, alternatively, collinear or in the form of an isosceles triangle). The trilinear coordinates for cases *(a)* and *(b)* correspond to points with numbers 1, 2 in figure 3a.

Let us consider the motion at $\mu = 1$, when the intensities of all three vortices are equal. The behavior of analogous vortex structures in a homogeneous fluid was exhaustively studied in [28], [10], [41].

Isolines of the Hamiltonian in trilinear coordinates for this case are shown in figure 2b.

Note that in this simplest case, the motions of vortices are also relatively simple and all belong to a single class {3}, where the lower-layer vortices are involved in rotation around one another, while the vortex $\binom{1}{1}$ can lie either within or outside the construction formed by them.

The phase portrait shows all motions to be periodic. Moreover, twice within each period, every evolving triangular structure degenerates into a collinear configuration and once takes the form of an isosceles triangle. A particular case of the collinear state can be the one when the upper-layer vortex lies precisely above one of the lower-layer vortices in the tangency points of the PR boundary with the lateral sides of the coordinate triangle: $t = (1.5,\ 0,\ 1.5)$ and $t = (1.5,\ 1.5,\ 0)$. The portrait contains two singular elliptic points. The upper point corresponds to a stable stationary state - a roundabout, when the vortices with subscripts $\binom{1}{2}$ and $\binom{2}{2}$, located symmetrically about the immovable central vortex of the upper layer, uniformly rotate along a circumference. The lower point corresponds to a structure in which merged lower-layer vortices rotate around a common center with a theoretically infinite angular velocity.

Figures 14.1.a–14.1.d illustrate the set of possible motions of such system in a sequence when passing from one experiment to another corresponds to the motion of the image point in the phase space along the boundary of PR from the upper polar singularity toward the lower polar singularity.

Figure 14.1.a shows a realization of a stationary roundabout. This is an example of absolute choreography. Obviously, the relative choreography (14.2.a) in the system of coordinates rotating with an angular velocity of peripheral vortices, is determined by three fixed points. Figure 14.1.b

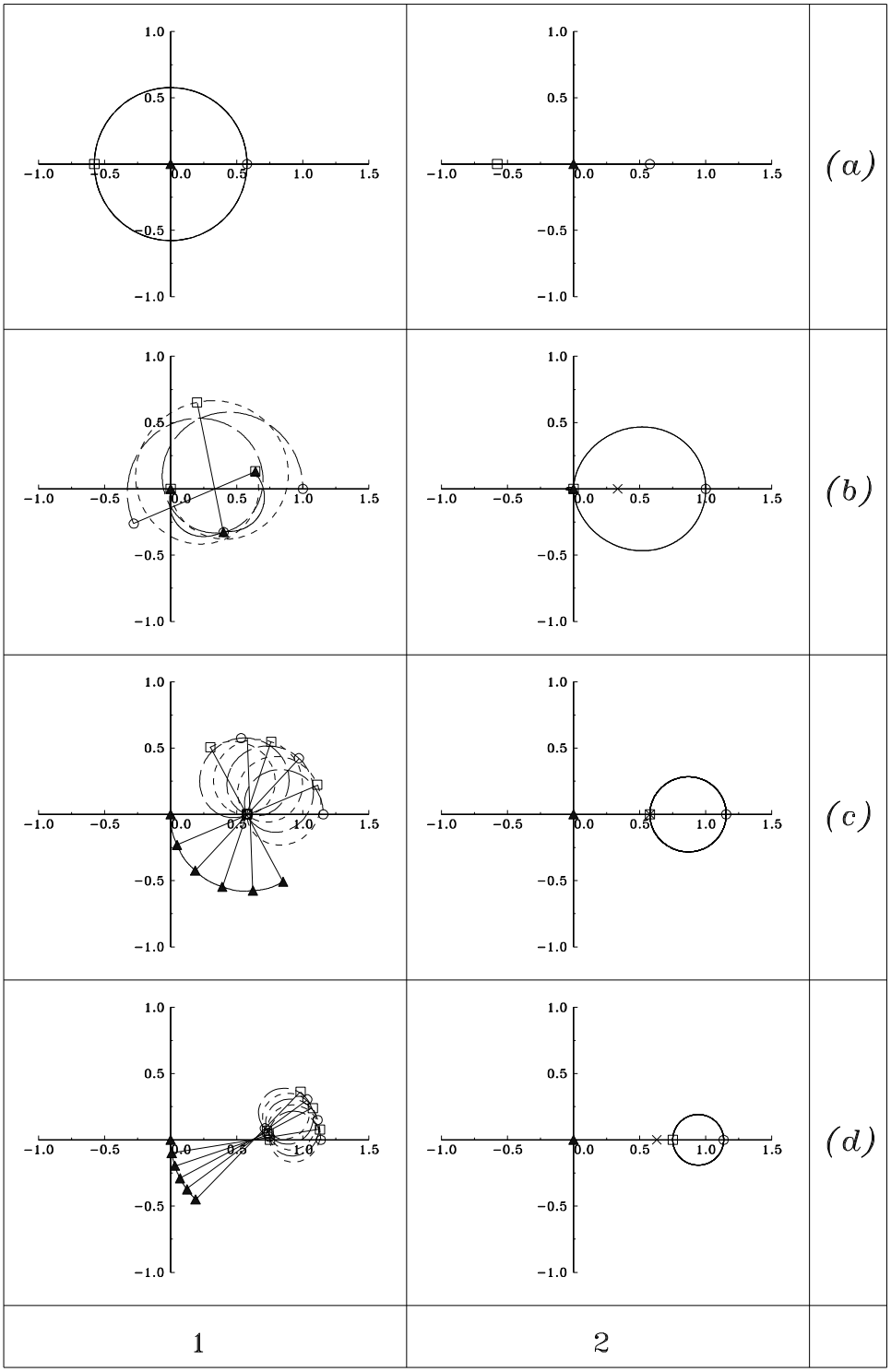

Fig. 14. 1 — Absolute trajectories of three vortices in the case $\mu = 1$ and $L = 2$. 2 — The respective relative choreographies in the coordinate system rotating in the cyclonic direction about the vorticity center of the system (its coordinates are marked by crosses). The initial conditions correspond to the following parameter values: *(a)* — $X_2^2 = -1/\sqrt{3}$, $t = (2.0, 0.5, 0.5)$ — point 1 in figure 2b; *(b)* — $X_2^2 = 0$, $t = (1.5, 0.0, 1.5)$ — point 2 in figure 2b; *(c)* — $X_2^2 = 1/\sqrt{3}$, $t = (0.5, 0.5, 2.0)$ — point 3 in figure 2b; *(d)* — $X_2^2 = 0.75$, $t = (0.2227, 0.8438, 1.9335)$ — point 4 in figure 2b.

shows the initial stage of the evolution of a vortex structure in the case when the vortices $\binom{1}{1}$ and $\binom{2}{2}$ coincide in the initial moment. The behavior of the system is such that the vortex periodically and alternatively coincides with the upper-layer vortices. This can be clearly seen in both the figures of relative trajectories (14.1.b) and relative choreographies (14.2.b). Figures 14.1.c and 14.1.d give the trajectories of absolute motion for the situations where vortex $\binom{1}{1}$ all the time stays out of the structure $\binom{1}{2}$-$\binom{2}{2}$. In the former case, the upper-layer vortices periodically coincide with the vorticity center of the system, and in the latter case, they alternatively change places always remaining on the same side with respect to this center.

Clearly, as the initial point of the phase trajectories moves farther toward the lower pole, the trajectories of the lower-layer vortices will describes a figure more and more similar to a circle with a radius tending to zero. This is also confirmed by the fact that the phase trajectories in the lower part of the figure are practically horizontal lines.

It should be mentioned that most examples considered above (figures 8, 11, 12, 14) represent the cases of compact PR. Now let us consider characteristic features of the absolute motions allowing for infinite trajectories. Suppose that $\mu = -1$. The respective phase portraits are given in figure 4.

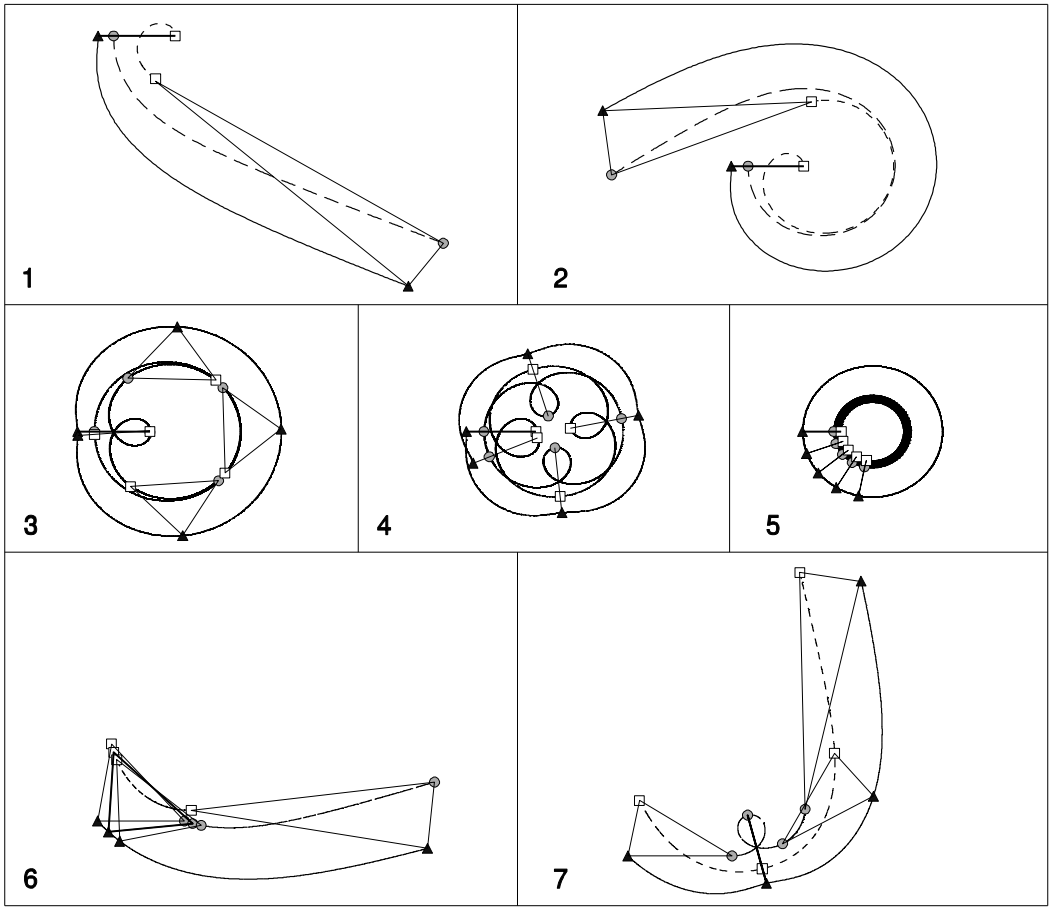

Fig. 15. Trajectories of absolute motion at $\mu = -1$, $\gamma^2 L = -2$ and the initial conditions corresponding to the enumerated points on the phase plane (figure 3b) with the following parameters: 1 — $X_2^2 = 0.45$, $t = (-4.7112;\ 7.4074;\ 0.3038)$; 2 — $X_2^2 = 0.4810$, $t = (-3.8304;\ 6.4824;\ 0.3770)$; 3 — $X_2^2 = 0.4811$, $t = (-3.3750;\ 6.0000;\ 0.3750)$; 4 — $X_2^2 = 0.5$, $t = (-4.7112;\ 7.4074;\ 0.3038)$; 5 — $X_2^2 = 0.9$, $t = (-0.0669;\ 1.8519;\ 1.2150)$; 6 — $X_2^2 = 2.5$, $t = (-15.0000;\ 8.6250;\ 9.3950)$; 7 — $X_2^2 = 3$, $t = (-15.0000;\ 4.5000;\ 13.5000)$.

Figure 15 gives mostly the initial parts of trajectories of absolute motion of vortices at $L < 0$. Experiments 1 and 2, demonstrating a realization of regime $\{2\}$, start from collinear initial configu-

rations. They show that mutual capture of vortices $\binom{1}{1}$ and $\binom{1}{2}$ takes place via the formation of a two-layer pair moving to infinity, whereas vortex $\binom{2}{2}$ at $t \to \infty$ takes some fixed position. In these figures, segments connect the positions of vortices in the initial and final moments of calculations.

Two more examples of infinite motions are given by experiments 6 (type $\{2\}$) and 7 (type $\{1\}$). Here, the initial structures are triangles (not isosceles), such that the distances r_{22}^{21} (or trilinear coordinates t_1) for these two cases are identical. In this case, obviously, coordinates Y_2^2 are chosen based on the conservation condition of invariant L. The configurations marked out in the first fragment are: a) initial, b) in the form of an isosceles triangle (corresponds to the image point lying on the line $t_2 = t_3$), c) the configuration antisymmetric to the initial one (in which the sides of the triangle with the lengths of r_{12}^{12} and r_{12}^{11} change places), and d) final. The configurations in the second fragment are the same with the exception that in item b), we have a collinear configuration (corresponding to the position of the image point on the PR boundary), and in item c), the configuration is symmetrical. Clearly, the possible class of vortex structures of motions of type $\{2\}$ includes the collinear state and does not include the configuration in the form of an isosceles triangle; the situation with motions of type $\{1\}$ is inverse.

Experiments 3, 4 and 5 demonstrate trajectories of finite type $\{3\}$ with a dominating character of intralayer interaction between lower-layer vortices $\binom{1}{2}$ and $\binom{2}{2}$[7].

Fragments 3–5 present trajectories in time intervals of $T/2$, $2T$ and $188T$ with marked out instantaneous configurations with intervals of $T/8$, $T/2$ and $12T$, respectively (T is the period of relative motion). Thus, motions of type $\{3\}$, as before, are represented by rotations along loop-like trajectories of cyclonic lower-layer vortices around some variable center. After each quarter of period, the vortex structure forms, in turn, either a collinear configuration or a configuration in the form of an isosceles triangle with successive rearrangement of vortices $\binom{1}{2}$ and $\binom{2}{2}$.

Figure 16 shows trajectories of absolute finite character (left) and the respective choreographies (right). Lines (a) and (c) correspond to figures 15.3 and 15.4, respectively. In both cases, the calculation time is extended (as compared with the previous figure) and amounts to about $6T$. The origin of coordinates coincides with the vorticity center of the vortex structure. During the construction of choreographies, the coordinate system was subjected to a rotational motion — counterclockwise in figure 16a and clockwise in figure 16c. It is clear that in this case, an intermediate state of the systems must exist when no rotation of the coordinate system is required and, thus, an absolute choreography is observed. This is the situation shown in figure 16b (the parameter values are given in the capture). The markers and the segments connecting them on the choreographies show the collinear and triangular positions of vortices with a time step of a quarter of the period.

Thus, in this case, as in the four-vortex problem with $P = 0$ and $M \neq 0$ [20], one of the phase trajectories in the class of finite motions $\{3\}$ is associated with an absolute choreography. It should be noted that this periodic solution is stable: the system of vortices in figure 16b has accomplished more than 20 cycles.

3. Conclusions

Possible motions of a system of three vortices were studied under the assumption that one vortex lies in the upper layer of a two-layer fluid and the other two vortices, which have equal intensities, lie in the lower layer. The associated dynamic system was studied in a wide range of external parameters. The relative motions were classified, in particular, dispersion relationships, determining the characteristics of stationary states, were obtained. A new stable stationary solution — *eccentric roundabout* was obtained; it generalizes the solution of *triton* type [40], [39] to the case of nonzero total intensity.

[7]Note that notwithstanding the fact that the initial conditions in experiments 2 and 3 are very similar (the markers with numbers 2 and 3 in figure 4 are practically indistinguishable), the respective motions belong to different types since the image points on the phase plane belong to trajectories lying in a vicinity of the separatrix but on different sides of it.

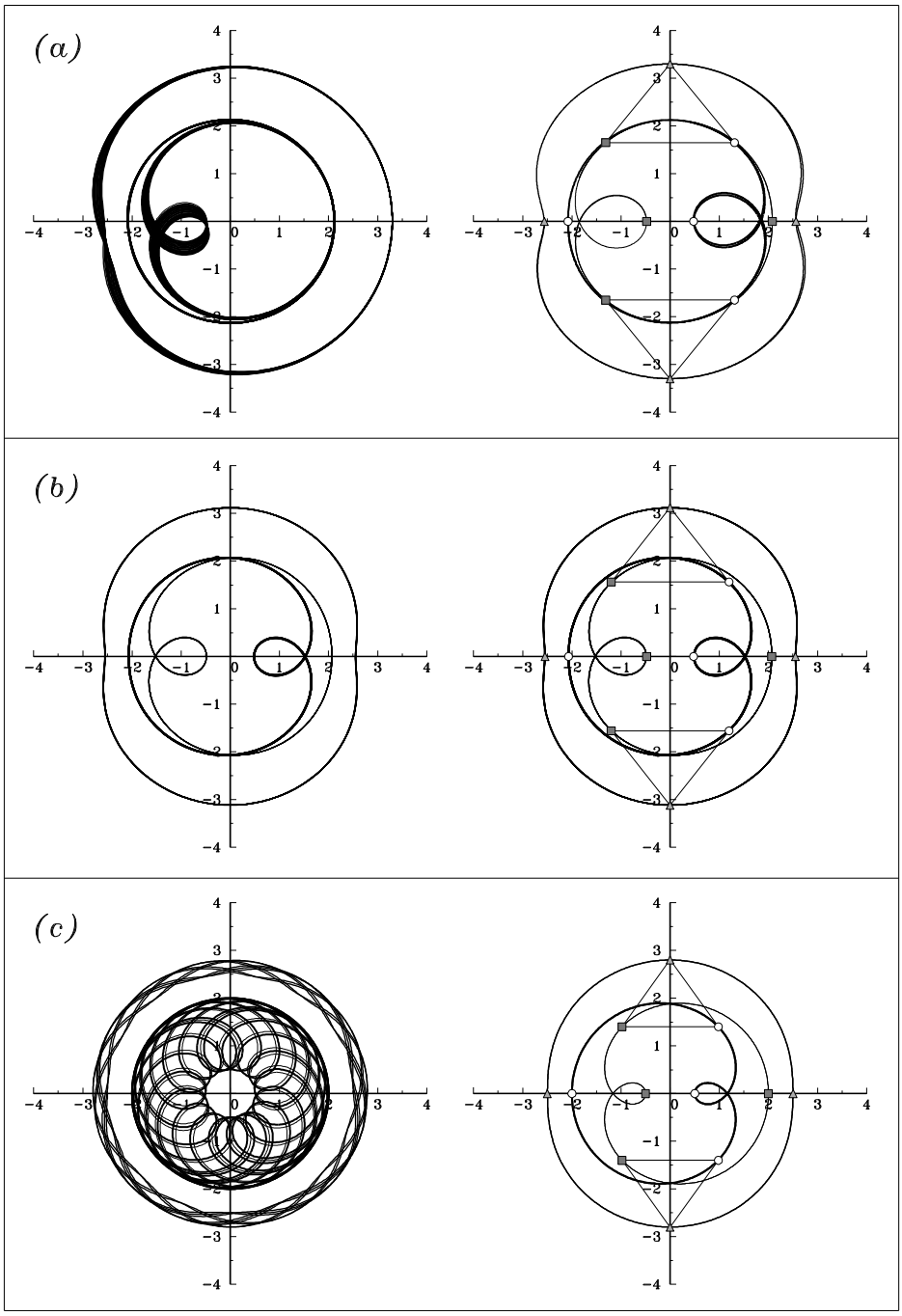

Fig. 16. Absolute trajectories of three vortices (left) and the respective choreographies (right) for motions of the type {3} at collinear initial state and the following parameter values: $\mu = -1$, $\gamma^2 L = -2$ and (a) — $X_2^2 = 0.4811$, $t = (-3.3750; 6.0000; 0.3750)$; (b) — $X_2^2 = 0.4833$, $t = (-3.7722; 6.4218; 0.3504)$; (c) — $X_2^2 = 0.5$, $t = (-4.7112; 7.4074; 0.3038)$.

The existence of relative and absolute choreographies for a system of three vortices was established. Numerically calculated absolute trajectories of vortices are exemplified. Clearly, these examples fail to reflect the entire spectrum of possible motions for the three-vortex system considered. However, the examples give an idea of their character. Additionally, the analysis of the presented phase portraits extends our knowledge about the properties of this dynamic system. In particular, the upper part of figure 4 (where $\gamma^2 L = 2$ and $\mu = -1$) shows that the respective symmetrical roundabout is *unstable*

(it corresponds to the bottom point of PR). The problem of stability of axisymmetric structures in the presence of a central vortex (in the manner of works [2], [10], [19], [27], [7], [16], [26], [30], but applied to a two-layer fluid medium) will be a subject of a separate paper.

The obtained results yield the explanation of some mechanisms of vortex interaction in a stratified rotating fluid and can be of use in the interpretation of specific features of real vortex structure trajectories in the ocean and atmosphere.

Acknowledgement

We are grateful to our colleagues V. M. Gryanik, A. V. Borisov and I. S. Mamaev for fruitful discussions of the results of this study. This work was financially supported by the Russian Foundation for Basic Research (project №04-05-64367).

References

[1] *H. Aref.* Motion of Three Vortices. Phys. Fluids. 1979. V. 22. №3. P. 393–400.

[2] *H. Aref.* Point Vortex Motions with a Center of Symmetry. Phys. Fluids. 1982. V. 25. P. 2183–2187.

[3] *H. Aref.* Integrable, Chaotic and Turbulent Vortex Motion in Two-Dimensional Flows. Annu. Rev. Fluid Mech. 1983. V. 15. P. 345–389.

[4] *H. Aref.* Three-Vortex Motion with Zero Total Circulation: Addendum. J. Appl. Math. Phys. (ZAMP). 1989. V. 40. P. 495–500.

[5] *H. Aref, S. W. Jones, S. Mofina, I. Zawadski.* Vortices, Kinematics and Chaos. Physica D. 1989. V. 37. P. 423–440.

[6] *H. Aref, M. A. Stremler.* Four-Vortex Motion with Zero Total Circulation and Impulse. Phys. Fluids. 1999. V. 11. №12. P. 3704–3715.

[7] *L. Bauer, G. K. Morikawa.* Stability of Rectilinear Geostrophic Vortices in Stationary Equilibrium. Phys. Fluids. 1976. V. 19. №7. P. 929–942.

[8] *M. Beckers, G. J. F. van Heijst.* The Observation of a Triangular Vortex in a Rotating Fluid. Fluid Dyn. Res. 1998. V. 22. P. 265–279.

[9] *A. V. Borisov, I. S. Mamaev.* Poisson Structures and Lie Algebras in Hamiltonian Mechanics. Izhevsk: Regular & Chaotic Dynamics. 1999. P. 464. (In Russian)

[10] *A. V. Borisov, I. S. Mamaev.* Mathematical Methods of Vortex Structure Dynamics. In: Fundamental and Applied Problems in the Theory of Vortices. (Eds. A. V. Borisov, I. S. Mamaev, M. A. Sokolovskiy). Moscow-Izhevsk: Institute of Computer Science. 2003. P. 17–178. (In Russian)

[11] *A. V. Borisov, A. E. Pavlov.* Dynamics and Statics of Vortices on a Plane and a Sphere. — I. Reg. & Chaot. Dyn. 1998. V. 3. №1. P. 28–39.

[12] *A. V. Borisov, V. G. Lebedev.* Dynamics of Three Vortices on a Plane and a Sphere. - II. General Compact Case. Reg. & Chaot. Dyn. 1998. V. 3. №2. P. 99–114.

[13] *A. V. Borisov, V. G. Lebedev.* Dynamics of Three Vortices on a Plane and a Sphere. - III. Noncompact Case. Problem of Collapse and Scattering. Reg. & Chaot. Dyn. 1998. V. 3. №4. P. 74–86.

[14] *A. V. Borisov, A. V. Bolsinov, I. S. Mamaev.* Lie Algebras in Vortex Dynamics and Celestial Mechanics. — IV. Reg. & Chaot. Dyn. 1999. V. 4. №1. P. 23–50.

[15] *A. V. Borisov, I. S. Mamaev, A. A. Kilin.* Absolute and Relative Choreographies in the Problem of Point Vortices Moving on a Plane. Reg. & Chaot. Dyn. 2004. V. 9. №2. P. 101–111.

[16] *H. E. Cabral, D. S. Schmidt.* Stability of Relative Equilibria in the Problem on $N + 1$ Vortices. SIAM J. Math. Anal. 1999. V. 31. №2. P. 231–250.

[17] *G. F. Carnevale, R. C. Kloosterziel.* Emergence and Evolution of Triangular Vortices. J. Fluid Mech. 1994. V. 259. P. 305–331.

[18] *V. M. Gryanik.* Dynamics of Singular Geostrophic Vortices in a Two-Layer Model of the Atmosphere (Ocean). Izvestia, Atmos. Oceanic Phys. 1983. V. 19. №3. P. 227–240. (In Russian) P. 171–179. (English translation)

[19] *V. M. Gryanik.* About Theoretical Models of Localized Quasi-Geostrophic Vortices in the Atmosphere and Ocean. In: The Investigations of Vortex Dynamics and Energetics of the Atmosphere and Climate. (Eds. E. G. Nikiforov, V. F. Romanov). Leningrad: Gidrometeoizdat. 1990. P. 31–60. (In Russian)

[20] *V. M. Gryanik, M. A. Sokolovskiy, J. Verron.* Dynamics of Baroclinic Vortices with Zero Total Intensity (Hetons). In: Fundamental and Applied Problems in the Theory of Vortices. (Eds. A. V. Borisov,

I. S. Mamaev, M. A. Sokolovskiy). Moscow-Izhevsk: Institute of Computer Science. 2003. P. 547–622. (In Russian)

[21] *G. J. F. van Heijst, R. C. Kloosterziel.* Tripolar Vortices in a Rotating Fluid. Nature. 1989. V. 338. P. 569–571.

[22] *G. J. F. van Heijst, R. C. Kloosterziel, C. W. M. Williams.* Laboratory Experiments on the Tripolar Vortex in a Rotating Fluid. J. Fluid Mech. 1991. V. 225. P. 301–331.

[23] *A. Hénon.* Family of Periodic Solutions of the Planar Three-Body Problem and Their Stability. Cel. Mech. 1976. V. 13. P. 267–285.

[24] *R. C. Kloosterziel, G. J. F. van Heijst.* On Tripolar Vortices. In: Mesoscale/Synoptic Coherent Structures in Geophysical Turbulence. (Eds. J. C. J. Nihoul, B. M. Jamart). Amsterdam - Oxford - New York - Tokyo: Elsevier. 1989. P. 609–625.

[25] *V. V. Kozlov.* Dynamical Systems X. General Theory of Vortices. Ser. Encyclopaedia of Mat. Sci. V. 67. Springer-Verlag. 2003.

[26] *L. G. Kurakin, V. I. Yudovich.* The Stability of Stationary Rotation of a Regular Vortex Polygon. Chaos. 2002. V. 12. №3. P. 574–595.

[27] *L. G. Kurakin, V. I. Yudovich.* Stability of Stationary Rotation of a Regular Polygon. In: Fundamental and Applied Problems in the Theory of Vortices. (Eds. A. V. Borisov, I. S. Mamaev, M. A. Sokolovskiy). Moscow-Izhevsk: Institute of Computer Science. 2003. P. 238–299. (In Russian)

[28] *V. V. Meleshko, M. Yu. Konstantinov.* Dynamics of Vortex Structures. Kiev: Naukova Dumka. 1993. P. 280. (In Russian)

[29] *C. Moore.* Braids in Classical Dynamics. Phys. Rev. Lett. 1993. V. 70. №24. P. 3675–3679.

[30] *G. K. Morikawa, E. V. Swenson.* Interacting Motion of Rectilinear Geostrophic Vortices. Phys. Fluids. 1971. V. 14. №6. P. 1058–1073.

[31] *L. M. Polvani, X. J. Carton.* The Tripole: A New Coherent Vortex Structure of Incompressible Two-Dimensional Flows. Geophys. Astrophys. Fluid Dyn. 1990. V. 51. P. 87–102.

[32] *A. P. Prudnikov, Yu. A. Brychkov, O. I. Marichev.* Integrals and Series. V. 2. Special Functions. N.-Y.: Gordon & Breach Sci. Publ. 1990.

[33] *N. Rott.* Three-Vortex Motion With Zero Total Circulation. J. Appl. Math. Phys. (ZAMP). 1989. V. 40. P. 473–494.

[34] *N. Rott.* Constrained Three- and Four-Vortex Problems. Phys. Fluids. 1990. V. A 2. №8. P. 1477–1480.

[35] *A. Chenciner, R. Montgomery, C. Simó, G. Gerver.* Simple Choreographic Motions of N Bodies: a Preliminary Study. In: Geometry, Mechanics, and Dynamics. Volume in Honor of the 60th Birthday of J.E. Marsden, (Eds. P. Newton, P. Holmes, A. Weinstein). New York: Springer. 2002. P. 287–308.

[36] *C. Simó.* New families of solutions in N-body problem. In: Proc. ECM 2000, Barcelona. Progress in Mathematics. Birkhäuser Verlag. 2000. V. 201. P. 101—115.

[37] *C. Simó.* Dynamical Properties of the Figure Eight Solution of the Three-Body Problem. Contemp. Math. V. 292, 209–228.

[38] *M. A. Sokolovskiy, J. Verron.* Four-Vortex Motion in the Two Layer Approximation: Integrable Case. Reg. & Chaot. Dyn. 2000. V. 5. №4. P. 413–436.

[39] *M. A. Sokolovskiy, J. Verron.* Dynamics of the Triangular Two-Layer Vortex Structures with Zero Total Intensity. Reg. & Chaot. Dyn. 2002. V. 7. №4. P. 435–472.

[40] *M. A. Sokolovskiy, J. Verron.* New Stationary Solutions to the Problem of Three Vortices in a Two-Layer Fluid. Russian Acd. Nauk. Doklady. 2002. V. 383. №1. P. 61–66. (In Russian) Doklady Physics. 2002. V. 47. №3. P. 233–237. (English translation)

[41] *J. Tavantzis, L. Ting.* The Dynamics of Three Vortices Revisited. Phys. Fluids 1988. V. 31. №6. P. 1392–1409.

[42] *O. U. Velasco Fuentes, G. J. F. van Heijst, N. P. M. van Lipzing.* Unsteady Behaviour of a Topography-Modulated Tripole. J. Fluid Mech. 1996. V. 307. P. 11–41.

[43] *S. L. Ziglin.* Nonintegrability of the Problem on the Motion of Four Point Vortices. Acad. Nauk SSSR Doklady. 1980. V. 250. №6. P. 1296–1300. (In Russian)